BUTTERWORTH HEINEMANN

REVIEW

Embedded vortices in internal flow: heat transfer and pressure loss enhancement

Martin Fiebig
Institut für Thermo- und Fluiddynamik, Ruhr-Universität, Bochum, Germany

Vortices depend strongly on the way they are generated. A class of wing-type vortex generators, which can easily be incorporated into heat transfer surfaces, is considered in fully developed and developing channel flows with respect to heat transfer enhancement and pressure loss penalty. Such configurations have been investigated in detail by the research group "Vortices and Heat Transfer" at the ITF of the Ruhr University. Three enhancement mechanisms are identified and discussed quantitatively: (1) developing boundary layers on the vortex generator surface; (2) swirl; and (3) flow destabilization. Experiments and calculations show that (1) winglets are more effective than wings, and (2) rectangular and delta winglets give similar performance. A base configuration with rectangular vortex generators is investigated in detail. Transition starts at Reynolds numbers below 300, and no dominant frequencies can be detected at Re = 1,000. At all Reynolds numbers, longitudinal vortices are more effective than transverse vortices; i.e., longitudinal vortex generators generate higher heat transfer enhancement for the same pressure penalty than transverse vortex generators.

Keywords: vortices; vortex generators; transition; heat transfer enhancement; pressure loss penalty; internal flow

Introduction

An agreed-upon mathematical definition of a vortex in a three-dimensional 3-D flow does not exist (Trefethen and Panton 1990). Nevertheless, everyone seems to know what a vortex is: a swirling flow around an axis of rotation. Vortices are generated by fluid friction and separation; therefore, to generate specific vortices, special surfaces are needed. These are called vortex generators, turbulence promoters, or sometimes turbulators. When they have the same scale as the viscous sublayer, they are also called roughness elements. Vortices have two features which enhance transport processes: they swirl and destabilize the flow field, so that a steady laminar flow will become highly instationary or turbulent (Ghaddar et al. 1986; Karniadakis et al. 1988; Grosse-Gorgemann et al. 1993).

Principally, transverse and longitudinal vortices can be distinguished. The axis of a transverse vortex lies perpendicular to the flow direction. A purely two-dimensional 2-D flow is possible. The Karman vortex street behind an infinite circular cylinder in cross-flow is the classical example of a transverse vortex system. Up to Reynolds numbers based on the diameter of about 40, the separation is symmetric, and the flow field is stationary. In the wake, there are two symmetric vortices, a recirculation zone, and a stagnation point. At Reynolds numbers above 40, vortex shedding starts (van Dyke 1988). Flow separation alternates between the sides of the cylinder, and the shear layers roll up to transverse vortices. The Strouhal number, a dimensionless shedding frequency, is 0.18 and does not depend strongly on Reynolds number. For transverse vortices, part of the induced or secondary flow is always in the direction opposite to the primary flow and leads to reverse flow behind the cylinder, when the cylinder is placed near a wall.

Longitudinal vortices have their axes parallel to the primary flow direction. The flow spirals around the main flow direction and is always three-dimensional 3-D. The induced flow can be of the same order of magnitude as the primary flow. The slender delta wing at an angle of attack is the classical example of a longitudinal vortex generator. The separation along the leading edges of the delta wing at an angle of attack is caused by the pressure difference between the upper and lower side. The separated shear layers roll up to a pair of counter-rotating, longitudinal vortices. Figure 1 from Delerey et al. (1984) shows three important features: (1) the longitudinal vortices may also become unstable and burst or breakdown when the angle of attack becomes too large, or when the vertex angle becomes too large; (2) the axial velocity in the core is about twice the free-stream value before vortex breakdown and becomes locally reversed after breakdown; and (3) the circumferential velocity is of the same order of magnitude as the free-stream velocity before vortex breakdown and becomes much smaller after breakdown. Vortex breakdown as seen in Figure 1 is connected with instability and unsteadiness of the flow.

It should be mentioned that it is impossible to generate pure longitudinal vortices. Transverse vortices are always generated at the same time. Vortices embedded in external flow have been studied very intensively because of their importance in aeronau-

Address reprint requests to Prof. Martin Fiebig, Institut für Thermo- und Fluiddynamik, Ruhr-Universität, 44780, Bochum, Germany.

Received 23 January 1995; 22 March 1995

Int. J. Heat and Fluid Flow 16: 376–388, 1995

655 Avenue of the Americas, New York, NY 10010

0142-727X/95/$10.00
SSDI 0142-727X(95)00043-P

tics, see for example, Hummel (1979), Leibovich (1984), and Sarpkaya (1989). They generate the lift needed for flying.

In comparison much less is known about vortices embedded in internal flows, although many different vortex generators have been used (Webb 1987). Their purpose is to generate vortices which increase heat transfer or mass transfer. Because of the far-reaching analogy between heat and mass transfer, most of the heat transfer results hold also for mass transfer when similar boundary conditions exist. Therefore, only heat transfer is considered here. A vortex generator causes not only additional heat transfer but also dissipation, or pressure loss. For compact heat exchangers, it has been shown that wing-type vortex generators are very effective heat transfer augmentation devices (Fiebig 1993). Figure 2 shows four basic wing-type vortex generators of identical area. Their attractiveness lies in the fact that the type and strength of the vortices can be controlled by the wing form and angle of attack. When the angle of attack is small, mainly longitudinal vortices are generated. When the angle of attack is 90°, mainly transverse vortices are generated. Therefore, the influence of the vortex type on flow structure, pressure loss, and heat transfer can be studied by changing the angle of attack. Wing-type vortex generators are considered here. For turbulent flow, the thermal resistance of the core region is low, and the major resistance lies in the viscous sublayer. When the vortex generator is of the size of the sublayer only the channel side where they are attached is influenced. We can speak of a

Notation

A	heat transfer surface
A_F	minimal free cross section
A_{fr}	frontal cross section
a	thermal diffusivity
B	width
B_P	lateral pitch
c	specific heat
D	pressure drag
d	diameter
d_h	hydraulic diameter, $(4 \cdot V/A) = (4 \cdot A_{\mathrm{E}}/P)$
e	rectangular fin height
f	frequency
H	channel height
$H(f)$	power density, Fourier transform
h	fin height
L	length
L_P	longitudinal pitch
l	fin length
P	perimeter
p	pressure
$\dot{q}$	heat flux
s_P	pivot point
T	temperature
t	time
U	mean axial velocity
u	axial velocity
v	lateral velocity
w	vertical velocity
x	axial coordinate
y	lateral coordinate
z	vertical coordinate

Greek

α	heat transfer coefficient
β	angle of attack
δ	fin thickness
λ	thermal conductivity
ν	kinematic viscosity
ρ	mass density
Φ	specific dissipation

Superscripts

*	dimensional quantity
$\bar{}$	averaged

Subscripts

air	fluid (air)
B	Bulk
conv	convective
d_h	hydraulic diameter
el	electrical
l	length
m	mean
max	maximum
min	minimum
p	pivot
t	tangential
VG	vortex generator
wall	wall
w	wall
rad	radiative
ref	reference
0	reference of flat plate

Dimensionless parameters

$$\mathrm{Nu} = \frac{\alpha^* \cdot d_h^*}{\lambda^*} = \frac{\partial T^*/\partial z^*\,|_w \cdot d_h^*}{(T_B^* - T_w^*)}$$ Nusselt number

$$\mathrm{Pr} = \frac{\upsilon^*}{a^*}$$ Prandtl number

$$\mathrm{Re} = \frac{\bar{u}^* \cdot d_h^*}{\upsilon^*}$$ Reynolds number

$$\mathrm{S} = \frac{f^* \cdot d_h^*}{\bar{u}^*}$$ Strouhal number

$$\mathrm{j} = \frac{\mathrm{Nu}}{\mathrm{Re} \cdot \mathrm{Pr}^{1/3}}$$ Colburn factor

$$\mathrm{c_f} = \frac{\tau_w^*}{\frac{\rho^*}{2} \cdot (\bar{u}^*)^2}$$ friction coefficient

$$\mathrm{c_D} = \frac{D^*}{\frac{\rho^*}{2} \cdot (\bar{u}^*)^2 \cdot A_{fr}^*}$$ form drag coefficient

$$\mathrm{c_\varphi} = \frac{\Phi^* \cdot 2H^*}{\Delta x^* \cdot (\bar{u}^*)^2}$$ dissipation coefficient

$$\mathrm{f} = \frac{\Delta p^*}{\frac{\rho^*}{2} \cdot (\bar{u}^*)^2} \cdot \frac{A_F^*}{A^*}$$ apparent friction factor

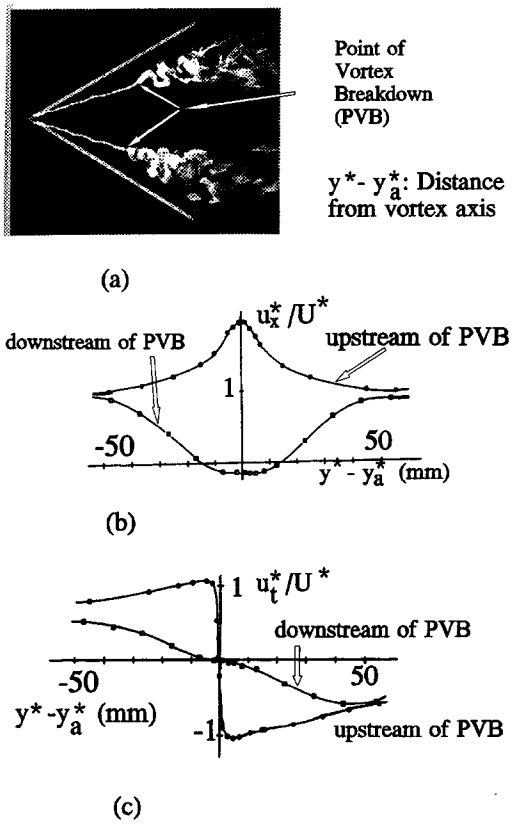

Figure 1 Breakdown of a pair of longitudinal vortices above a triangular wing; (a) a thin wing of equilateral planform is seen from above at 20° angle of attack in a water tunnel; the Reynolds number is 5000 based on the chord of 10 cm; filaments of colored fluid show that the pair of laminar vortices that roll up from separation at the leading edges abruptly burst into pockets of turbulent fluid; ONERA photograph, Werle, from van Dyke (1988); (b) axial and (c) tangential velocity components upstream (−50 mm) and downstream (120 mm) of vortex breakdown, $(y - y_a)$ distance from vortex axis, Delerey et al. (1984)

roughness element (Kozlu et al. 1988). There is an extensive literature on heat transfer enhancement by roughness. Surveys are given by Bergles and Webb (1985) and Webb. When the height of the vortex generator is comparable with the channel height, both sides are influenced.

Wing-type vortex generators shown in Figure 2 are called wings when their span is attached to the wall and winglets when

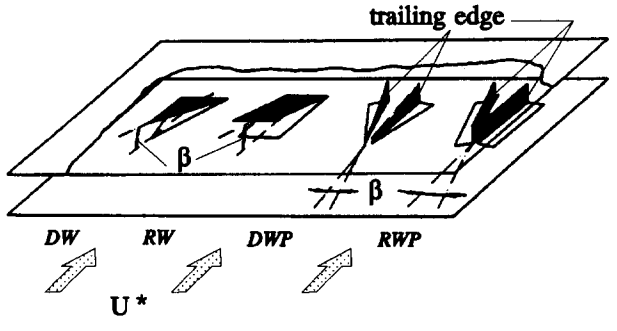

Figure 2 Basic wing-type vortex generators (WVG) investigated

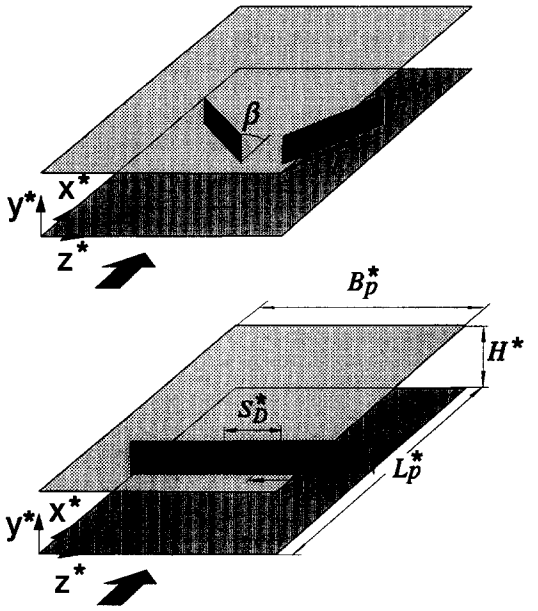

Figure 3 Base configuration with vortex generators at angle of attack of 45° and 90°; periodic channel element with a pair of attached plates at angle of attack; dimensionless parameters are longitudinal and lateral pitch $L_P = 5$, $B_P = 4$: length-, height-, and thickness-ratio of $l = 2$, $h = 0.5$, $\delta = 0.07$ and varying angle of attack β with point of rotation $s_D = l/2$; all lengths are made dimensionless with H^*

their chord is attached to the wall (Fiebig et al. 1986). Extensive experimental and numerical investigations of delta and rectangular wings and winglets were performed by Fiebig et al. (1991), Güntermann (1992), Kallweit (1986), Tiggelbeck (1990), Tiggelbeck et al. (1993), Zhang (1989), Zhu (1991), and Zhu et al. (1993, 1994). They compared different wing and winglet vortex generators. They found that the differences between rectangular and triangular winglets with regard to pressure penalty and heat transfer enhancement are small. However, winglets give higher heat transfer enhancement and lower pressure loss penalty than wings. Here mainly rectangular winglets attached to a wall, as shown in Figure 3, are considered. The single shape still leaves six variable geometric parameters. The base geometry selected and shown in Figure 3 fixes the longitudinal and lateral pitch to $L_p = 5$, $B_P = 4$, the length, height, and thickness ratio to $l = 2$, $h = 5$, and $\delta = 0.07$, and the point of rotation to $s_p = 1$. All lengths are nondimensionalized with the channel height H^*. All dimensional quantities have an asterisk as a superscript. The main geometrical parameter that is varied is the angle of attack β. Because the lateral pitch B_P equals 21, a continuous rib is formed for $\beta = 90°$.

The objective of this paper is to discuss the effects of vortices on heat transfer and pressure loss in transitional and turbulent flows when the vortices are generated under controlled conditions. Transition starts when the first self-sustained finite amplitude oscillation is generated in the flow, and turbulence is reached when, for practical purposes, a continuous spectrum of frequencies exists. I draw heavily on results of our research group "Vortices & Heat Transfer" at the Institute of Thermo- & Fluid Dynamics of the Ruhr-University, which is financed by the Deutsche Forschungsgemeinschaft (DFG). In the next section, different heat transfer enhancement mechanisms and the associated pressure loss penalties, which occur in connection with wing-type vortex generators, are presented. Then the numerical and experimental methods used by our group for the investigation

of vortex flows is briefly described. Afterward, results of heat transfer enhancement and pressure loss for vortex generators in transitional and turbulent channel flow are presented. The paper closes with some concluding remarks.

Enhancement mechanisms

Heat transfer enhancement means that heat transfer from or to the wall is increased over its normal value, here, the corresponding plane channel value. It implies enhanced temperature gradients at the wall. Three heat transfer enhancement mechanism are commonly used by passive enhancement techniques: (1) developing boundary layers; (2) swirl; and (3) flow destabilization. All three mechanisms can be induced by the rectangular vortex generators of the periodic element of Figure 3, which can be considered as an element of a 3-D array of such elements in a finned plate heat exchanger. Two angles of atack of the vortex generators $\beta = 45°$ and $\beta = 90°$ are shown. For $\beta = 45°$, mainly longitudinal vortices are generated. For $\beta = 90°$, when the vortex generator forms continuous transverse ribs (for the geometry of Figure 3), mainly transverse vortices are generated.

Heat transfer enhancement due to vortex generators is associated with pressure loss enhancement. The enhanced pressure losses are due to form drag of the vortex generators, changes of the wall shear, and, in nonperiodic situations, changes in the momentum flux.

First, the enhancement mechanism of developing boundary layers is considered. New boundary layers are generated on each side of the rectangular winglet, (if the vortex generators are stamped, additional boundary layers form at the stampings). For turbulent channel flow, the developing boundary layers on the winglets will be turbulent, otherwise they will be laminar. With the broad assumptions (1) that a turbulent (laminar) flat plate boundary layer develops on each side of a vortex generator; (2) that the outer flow may be approximated by the mean channel velocity; and (3) that the wake completely dissipates the boundary layers, the equations for developing turbulent (laminar) flat plate boundary layers can be used to estimate the enhancement over the fully developed channel flow values. With the Colburn analogy, valid for flat plate external flow

$$2j = c_f \tag{1}$$

and the assumption $\mathrm{Pr} \approx 1$ for the fully developed channel flow, the following equations for turbulent and laminar flat plate and fully developed channel flow hold (Bhatti and Shah 1987; Merker 1987):

Turbulent:

Flat plate:

$$2j = c_f = 0.074\ \mathrm{Re}_l^{-0.2} \tag{2}$$

Channel:

$$j = 0.0214\ \mathrm{Re}_{dh}^{0.2} - \frac{100}{\mathrm{Re}_{dh}} \tag{3}$$

$$c_f = 0.046\ \mathrm{Re}_{dh}^{-0.2} \tag{4}$$

Laminar:

flat plate:

$$2j = c_f = 1.328\ \mathrm{Re}_l^{-1.2} \tag{5}$$

channel:

$$j = 7.54\ \mathrm{Re}_{dh}^{-1} \tag{6}$$

$$c_f = 24\ \mathrm{Re}_{dh}^{-1} \tag{7}$$

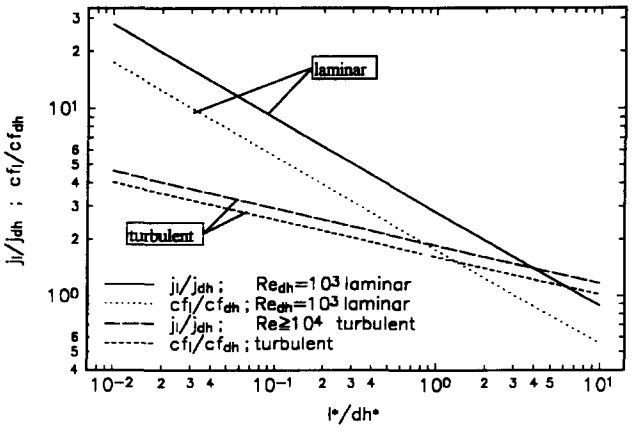

Figure 4 Enhancement of heat transfer and friction due to developing flow, ratio of flat plate values over fully developed channel values in laminar and turbulent flow

For the pressure loss, the form drag of the vortex generator—here, the plate—must be taken into account. With the form drag coefficient $c_D \sim 1$, the apparent friction factor f for zero angle of attack and for two sides of the plate is

$$f = 2c_f + c_D\frac{t}{l} \approx 2c_f + \frac{t}{l} \tag{8}$$

Equations 2–4 and 5–7 show that the enhancement effect of developing boundary layers is much more pronounced in laminar than in turbulent flow, except when the development length becomes larger than the hydraulic diameter (Figure 4). In the configuration of Figure 3, $l = d_h$. For the vortex generator at an angle of attack of 45°, the c_f and Nu values are not identical on the pressure and suction side and different from the flat plate values. The form drag will be proportional to the projected area. The enhancement of friction and heat transfer has been numerically calculated for a Reynolds number of 350 by Müller (1994). It was found that for the geometry of Figure 3 with $\beta = 45°$, the mean heat transfer increases by a factor of 1.8 over the fully developed channel values. When the wall area is much larger than the vortex generator area, in our example $A_w/A_{VG} = 10$, developing boundary layers on the vortex generators are not the dominating enhancement effect.

Enhancement by swirl is the most important mechanism in steady flow. To separate the swirl effect from the destabilization effect of the vortices the flow has to be steady. The vortices generated by flow separation along the side edge of each rectangular plate swirl the flow. The strength of the swirling flow can be seen in Figure 5, where the secondary flow in different cross sections is shown for Re = 350 and angle of attack $\beta = 45°$. The circumferential velocity becomes as large as the average axial velocity, and the velocity field is strongly 3-D. The longitudinal vortices lead to a spiralling motion and an exchange of fluid between the wall layer and the core. This enhances the heat transfer mainly in the downwash region of the vortex; i.e., the stagnation region and the area of high cross-flow velocities. If symmetry conditions are imposed on the side boundaries of the periodic element, the flow is still steady at Re = 350 (Müller 1993). The 2-D heat transfer distribution on the upper and lower wall are shown in Figure 6. On the wall where the vortex generators are attached, the increase in heat transfer is especially strong in the downwash region of the two counter-rotating longitudinal vortices. On the wall without vortex generators, the heat transfer distribution is more even. The mean value of the heat transfer enhancement on the upper and lower wall is 1.4. Therefore, it can be concluded that longitudinal vortices enhance heat

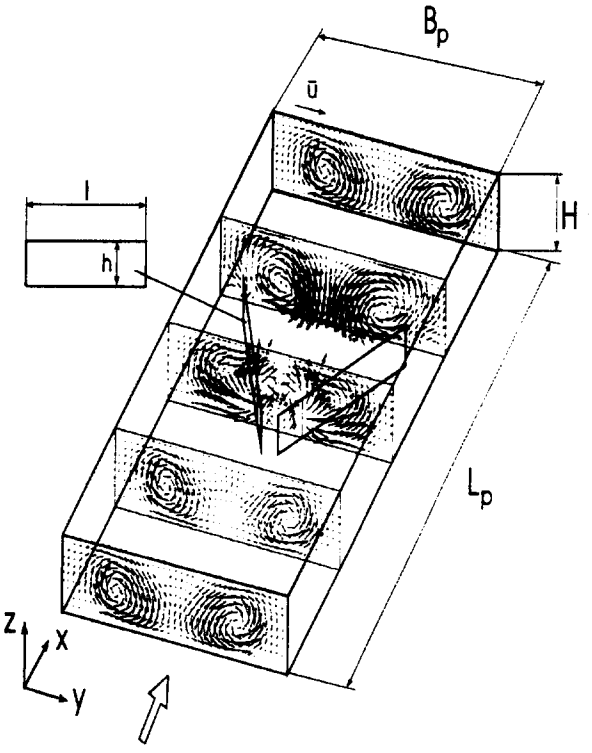

H = 1; B_p = 4; L_p = 5; l = 2; h = 0. ; nondimensionalized with H*

Figure 5 Counter-rotating longitudinal vortices; cross velocity vector plot of the induced cross-flow calculated for the base configuration of Figure 3 with β = 45° at Re = 350 from Müller (1993). The flow was steady, because symmetric side boundary conditions were enforced

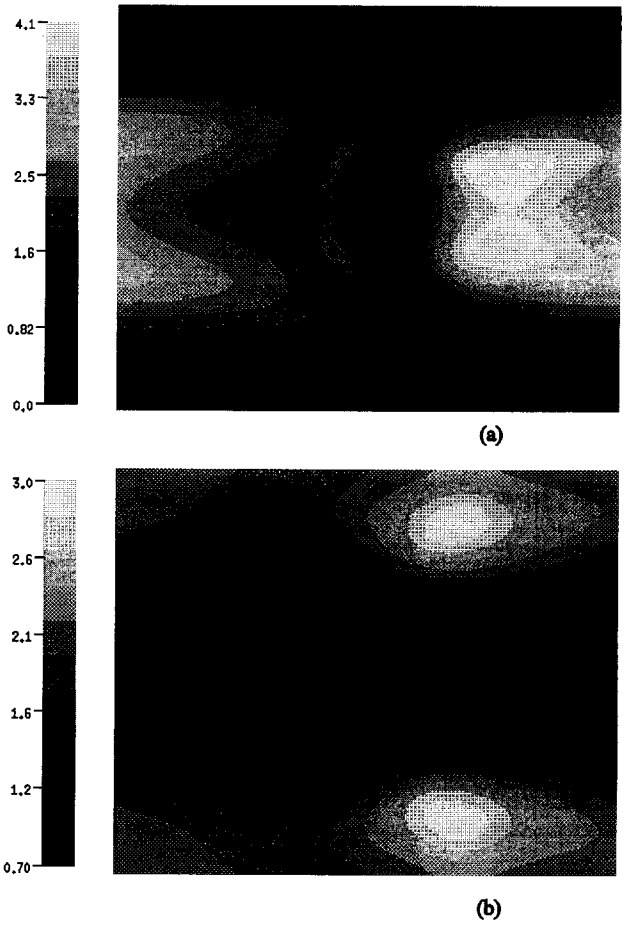

Figure 6 Nusselt number enhancement on the (a) lower and (b) upper wall relative to the fully developed channel flow values for the geometry and conditions of Figure 5, from Müller (1994)

transfer in steady flow. What is the situation for transverse vortices? So far no case has been reported where global heat transfer enhancement by transverse vortices has been observed in steady flow. Recently, Schäfer and Herwig (1993) reported that, for a laminar boundary layer with a finite region of separation, strong variations in local heat transfer and friction occurred, but no global changes in heat transfer or drag. For the ribbed channel of Figure 3 with β = 90°, no heat transfer enhancement could be detected as long as the flow was stationary, (Grosse-Gorgemann et al. 1993). However, an increased pressure loss occured despite the reduced friction on the walls. As long as the flow is steady, transverse vortices do not improve convective heat transfer from the walls to the main stream, since the transverse vortices with their steady 2-D flow have no convective mechanism for heat transfer enhancement. Therefore, in steady flow, only longitudinal vortices can increase heat transfer significantly by generating a 3-D spiralling motion, which transports heat convectively. The pressure penalty is, nevertheless, higher for the transverse vortex generator (β = 90°) than for the longitudinal vortex generator (β = 45°) of the same surface area.

The third mechanism, flow destabilization, is finally considered. For fully developed channel flow, the critical Reynolds number based on the hydraulic diameter is 15,392 for infinitesimal disturbences (Drazin and Reid 1984). However, the transverse vortex in the ribbed channel leads to a recirculation region and profiles with reversed flow. They are less stable, and their critical Reynolds number is much lower than the critical Re of fully developed channel flow. For the Falkner–Skan family of similar boundary layers, the profiles with reversed flow have a critical Reynolds number up to two orders of magnitude smaller than the critical Re of the Blasius profile. A similar result is obtained from the stability analysis of diffuser flows with regions of reversed flow (P. Schäfer, private communication, 1994). In an experimental study with hot wire measurements, Grosse-Gorgemann et al. (1994) have shown that for the geometry of Figure 3 the flow becomes unsteady at Re ≈ 200 for β = 90° and is already nonperiodic at Re = 350. Nonperiodic oscillations are also indicated by the frequency spectrum of the numerical results of Müller (1994). Figure 7 shows selected instantaneous streamlines once in the side-view projection and once in a top view. At Re = 350, five vortices appear in one spatial period, and they move along the channel and change with time. The top view shows the strong three-dimensionality of the flow field. A large number of frequencies appear in the frequency spectrum. The flow is transitional, and heat transfer from the wall is clearly increased by the convective transport due to the velocity component vertical to the wall. For the ribbed channel of Figure 3, this amounts at Re = 350 to an enhancement of 54%. With periodic side boundary conditions the wing-type vortex generator with 45° angle of attack leads to an oscillatory flow at Re = 350. The frequency spectrum is, however, narrower than that for the ribbed channel. Comparison of the steady solution for the same Re but different side boundary conditions, makes it possible to estimate the contribution of the flow unsteadiness to the heat transfer. Calculations show an increase of 12% over the steady value. In turbulent flow, it is not possible to separate the destabilization effect from the steady swirl effect. In general, such vortex

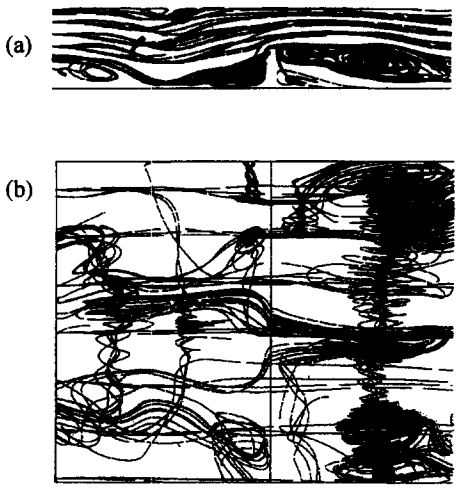

Figure 7 Instantaneous streamlines for the configuration of Figure 3, $\beta = 45°$ at Re = 350, (a) side view, (b) top view from Müller (1994). The strong three-dimensionality of the flow field at Re = 350 compared to the strict two-dimensionality at Re = 100 is noteworthy

generators should be selected which generate the highest longitudinal swirl and flow destabilization at a minimum pressure penalty.

Methods of investigation

Numerical methods

In the transitional regime, the numerical investigations were performed with a finite volume direct numerical simulation (DNS) of the 3-D unsteady Navier–Stokes equations, and the energy equation for a constant property Newtonian fluid, (Grosse-Gorgemann et al. 1993; Kost et al. 1992). For 2-D, unsteady grooved channel flow, the code has been validated with the spectral element code Nekton, which was provided by A. T. Patera (personal communication, 1991) and hotwire measurements by Grosse-Gorgemann et al. (1994). For 3-D unsteady flow grid refinement studies were performed to estimate the grid dependence of the results. For turbulent flow, a 3-D $k-\varepsilon$ model has been used (Zhu 1991; Zhu et al. 1993). For the smooth wall, the wall function of Launder and Spalding (1974) and for rib roughened walls the wall functions of Hanjalic and Launder (1972), Donne and Meyer (1977), and Han et al. (1978) were used. The code was validated with the experimental values of Hanjalic and Launder and the fully developed channel flow (Kakac et al. 1987). In addition, it was validated with 3-D experiments of Eaton and coworkers, who provided tapes of their experimental values of longitudinal vortices embedded in a turbulent boundary layer (Eibeck and Eaton 1986).

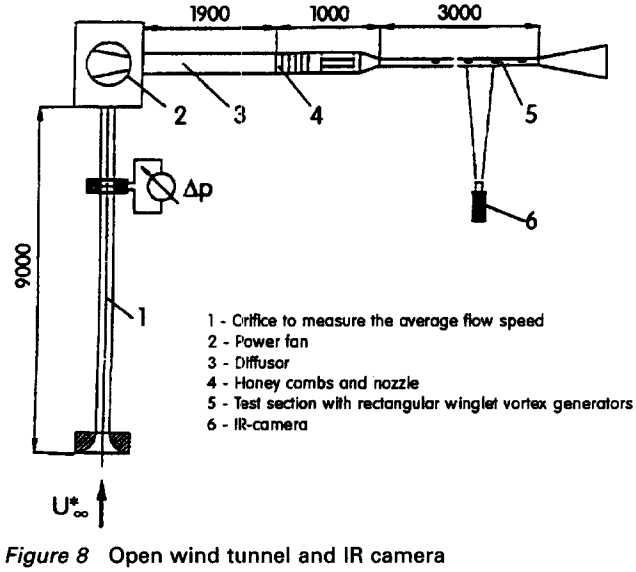

Figure 8 Open wind tunnel and IR camera

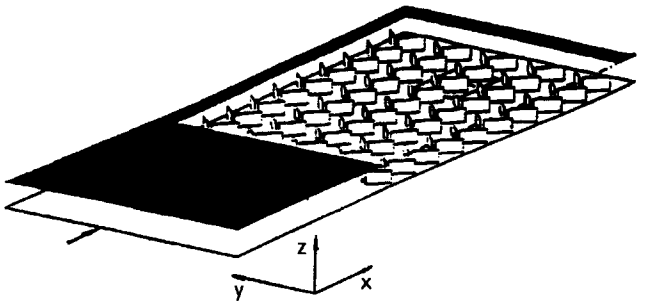

Figure 9 Test section with vortex-generators

Experimental methods

Local wall temperatures were determined either by infrared thermography (IRT) or by liquid crystal thermography (LCT). The IR-technique is documented in the thesis of Riemann (1992). He measures the Nusselt numbers with an accuracy of better than 6%. The fluid and thermal boundary conditions for the IR measurements were: (1) fully developed hydrodynamic conditions, and (2) constant heat flux thermal entrance conditions on the wall where the vortex generators were attached. The opposite wall was adiabatic and had an IR window. The vortex generators themselves were unheated. The wind tunnel and the IR camera is shown schematically in Figure 8. The test section is 3000-mm long to achieve a fully developed flow and has a cross section of 40×800 mm^2. Based on the hydraulic diameter of twice the channel height, Reynolds numbers between 10^3 and $5 \cdot 10^4$ could be realized. Ten rows of each ten vortex generators with $l^* = 80$ mm; $h^* = 20$ mm, $\delta^* = 2$ mm were installed in the test section (Figure 9). The vortex generators can rotate on their pivot to any desired angle of attack (Figure 10). Thus, the geometry corresponded completely to that of Figure 3, except for the little mismatch in δ^*. The constant heat flux was realized by a thin electrically heated copper foil. The heating was restricted to the area of one row of vortex generators. More precisely, the foil was put between the pivots of the 8th and the 9th row. Thus, the

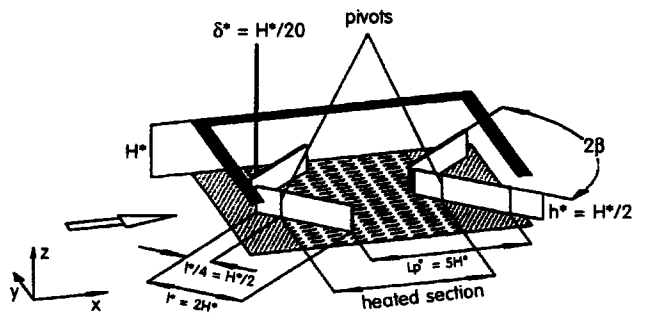

Figure 10 Winglet configuration and geometrical parameters, heated section between 8th and 9th row

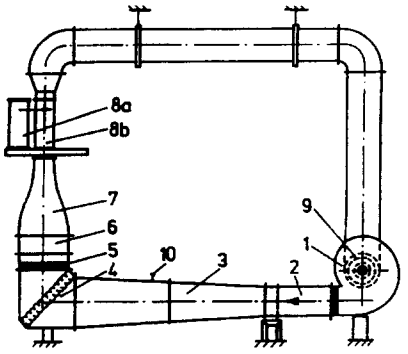

Figure 11 Closed thermal wind tunnel for liquid crystal thermography (LCT): 1, blower; 2, expansions; 3, wide-angle diffuser; 4, 90° turnaround; 5, straightener chamber; 6, mixing chamber; 7, nozzle; 8a, test section with model (160 mm×320 mm×800 mm); 8b, test section without model; 9, heater, 10, reference temperature sensor

length of the foil, limited by the distance between two pivots, was 4.85 H^*, which was slightly less than the full period length $5H^*$. Its width was $5H^*$. The heated area was made visible to the IR camera by a calcium fluoride window, which constituted the opposite channel wall. The 2-D temperature distribution was measured by an AVIO TVS 200 infrared camera. The local wall temperature T^*_{wall}, the fluid temperature T^*_{air}, and the convective heat flux $\dot{q}^*_{\text{conv}} = \dot{q}^*_{\text{el}} - \dot{q}^*_{\text{rad}}$ were used to calculate the local Nusselt number

$$\text{Nu} = \frac{2H^*(\dot{q}^*_{\text{el}} - \dot{q}^*_{\text{rad}})}{\lambda^*(T^*_w - T^*_{\text{air}})} \tag{9}$$

The static pressure along the channel was measured by an MKS Baratron.

For the liquid crystal thermography, a closed thermal wind tunnel was used where the air could be heated to 50°C (Figure 11). The test section of 800 mm length is designed to investigate entry flow conditions. For a hydraulic diameter of 40-mm, Reynolds numbers between 1,000 and 8,000 could be realized.

Liquid crystal thermography also needs optical visibility, so the model was built of polycarbonate. The test section and experimental apparatus for LCT is depicted in Figure 12. The wall at which the local heat transfer coefficient will be determined is coated with an LC; the experiment procedures as follows then. First, the test model at room temperature $T_0^* \approx 20°$ is suddenly slid into the wind-tunnel test section with $T^*_{\text{air}} = 50°\text{C}$, and the timer initiates the Argon laser and the camera. Second,

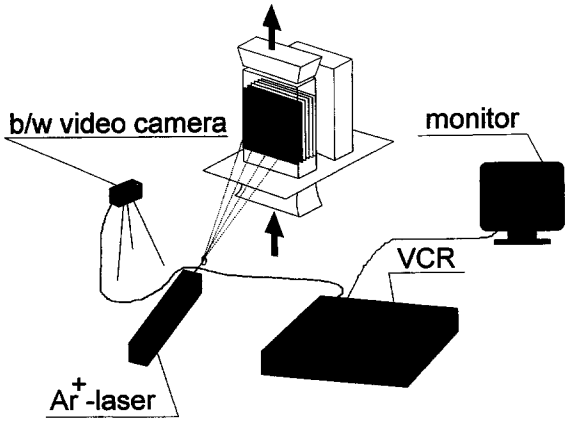

Figure 12 Test section and experimental setup for LCT

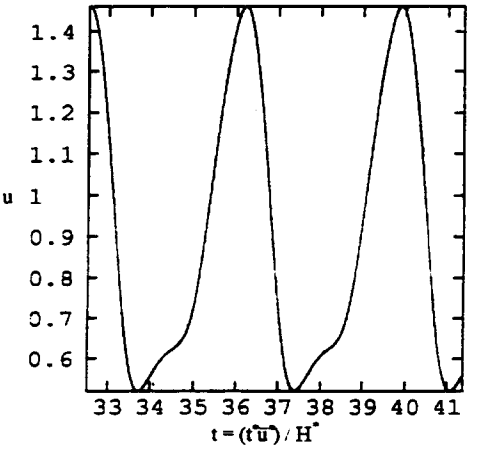

Figure 13 Time history of the axial velocity fluctuations for the base-geometry of Figure 3 with $\beta = 45°$: Re = 350 at $x = 0.1$, $y = 0.45$, $z = 0.6$ from Müller (1994). The origin of the coordinate system is at the lower left corner of a periodic element, the point of rotation is at $x = L_P/2$

the camera records the time history of the "green" temperature contour of the LC which correspondens to $T^*_w = 30.4°\text{C}$ for the used LC. Third, the local Nusselt number is determined by evaluation of the time history of the wall temperature $T^*_w(t^*, x^*, y^*) = 30.4°\text{C}$. In the thin film approximation, the Nusselt number is

$$\text{Nu} = \frac{\alpha^*(x, y)2H^*}{\lambda^*} = \frac{H^*\rho^*_w c^*_w \delta^*}{\lambda^* t^*} \ln\left[\frac{T^*_{\text{air}} - T^*_0}{T^*_{\text{air}} - T^*_w(t, x, y)}\right] \tag{10}$$

Here ρ^*_w, c^*_w, and δ^* are the density, specific heat, and thickness of the wall, respectively. Also t^* stands for the recorded time at which the temperature of the wall reaches 30.4°C, and $T^*_w(t^*, x^*, y^*)$ is the wall temperature, T^*_0 is the initial temperature of the wall, and T^*_{air} is the heated air temperature. The thin film assumption is equivalent to the constant temperature boundary condition. In contrast to the IR technique, here both walls have the same boundary condition. Tiggelbeck (1990) estimated the accuracy of the heat transfer coefficient to be better than 5%. The pressure loss was determined by a drag balance in a vertical wind tunnel with an accuracy of 10%.

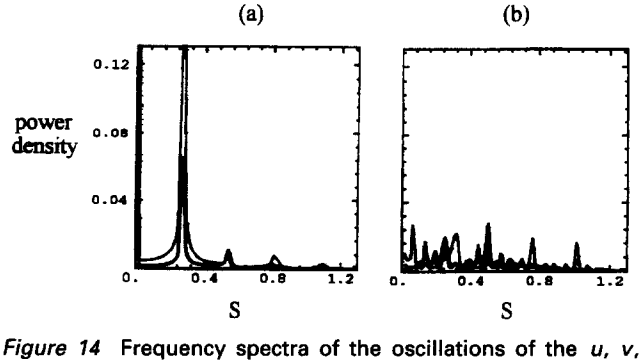

Figure 14 Frequency spectra of the oscillations of the *u*, *v*, and *w* velocities at point *P(x, y, z)* at Re = 350. (a) $\beta = 45°$ *P* (0.1, 0.45, 0.6); (b) $\beta = 90°$, *P*(0.45, 2.0, 0.6), from Müller (1994)

Results and discussion

The wing-type vortex generators for which results are presented are shown in Figure 2. Emphasis is placed on the winglet geometries. Two geometric parameters are varied—the wall to vortex generator area A_w/A_{VG} varies between 10 and 40, and the angle of attack β varies between 0° and 90°. Two flow situations are presented: fully developed periodic flow conditions and developing flow. The thermal boundary conditions are either constant wall temperature or constant heat flux at one wall and the other wall adiabatic. The Reynolds number varies between 350 and $3 \cdot 10^5$. At Re = 350, large self-sustained oscillations are present for fully developed periodic flow conditions and angles of attack of 30° and larger. These oscillations are part of the transition process. The critical Reynolds number is sharply reduced by the destabilizing effect of the vortices, which cause velocity profiles with inflection points and reversed flow. The strong geometric periodicity selects those frequencies from the Tolmien–Schlichting frequency spectrum, which have minimum damping. For entrance conditions with a single row of vortex generators, the feedback mechanism of the periodic geometry does not exist, and the critical Reynolds number is higher. For Re = 2200, the turbulence level behind a row of vortex generators reaches values higher than 10% when the initial turbulence level is below 1% (Tiggelbeck 1990).

Transitional flow conditions

First, numerical results for the fully developed flow conditions for the geometry of Figure 3 with $A_w/A_{VG} = 10$ and Re = 350 are discussed. The amplitudes and frequencies of the oscillations vary with the geometric position. For β = 45°, the axial velocity fluctuations are shown in Figure 13 as an example. For the point chosen in Figure 13, the mean axial velocity is $u_{ref} = 0.9$, and u varies between $u_{max} = 1.46$ and $u_{min} = 0.52$. For the other two components, not shown here, the corresponding values are $v_{ref} = 0.084$, $v_{max} = 0.182$, $v_{min} = -0.098$, and $w_{ref} = 0.107$, $w_{max} = 0.312$, $w_{min} = 0.039$. Thus, the axial fluctuations have an amplitude of half the mean velocity, the other velocity components have fluctuations of about 10% of the mean axial velocity and 100% of their own mean value. A Fourier analysis of the three velocity components shows that all components have the same frequency spectrum. Comparison of the frequency spectra for β = 45° and β = 90° (Figure 14) shows that for β = 90°, a dominant frequency does not exist, and the frequencies of the different velocity components are not identical. This result is also substantiated by hot-wire measurements at Re = 1,000, see Figure 15. A wide frequency spectrum occurs for β > 45°. The large peak at 50 Hz is introduced by the 50 Hz of the power supply. A dominating frequency does not exist, but the frequency spectrum is not yet as wide as in a fully turbulent flow. Space limitations do not permit examination of the details of the time-averaged local friction coefficients and Nusselt numbers. Therefore, only the time- and wall-averaged friction coefficient and Nusselt numbers normalized with their fully developed values are shown in Figures 16 and 17. The Re = 350, and the angle of attack is varied. The geometry corresponds to Figure 3. Symmetric and periodic side boundary conditions are considered. Both boundary conditions lead to steady flow for β ≤ 15° and to unsteady flow for β ≥ 60°. At 25 ≤ β ≤ 55, the flow is steady for symmetric boundary conditions and oscillatory for periodic side boundaries. The small influence of the fluctuations on the wall friction and also on the form drag of the winglets is evident in Figure 16. The pressure penalty due to form drag of the winglets becomes dominant for β ≥ 30°. For the heat transfer, a similar comparison can be made. In contrast to the c_f values, a marked increase in Nusselt Number as a result of the oscillations can be seen in Figure 17. The contributions of the oscillations to the heat transfer are especially large for β = 30°. Here the lateral extent of the longitudinal vortices is still small, and the lateral oscillations extend the lateral range of the vortices considerably. For β ≤ 25° and β ≥ 55°, the differences between the different boundary conditions become negligible.

For hydrodynamically and thermally developing flow, Tiggelbeck (1990) performed extensive experimental investigations of one row of wing-type vortex generators. He investigated delta

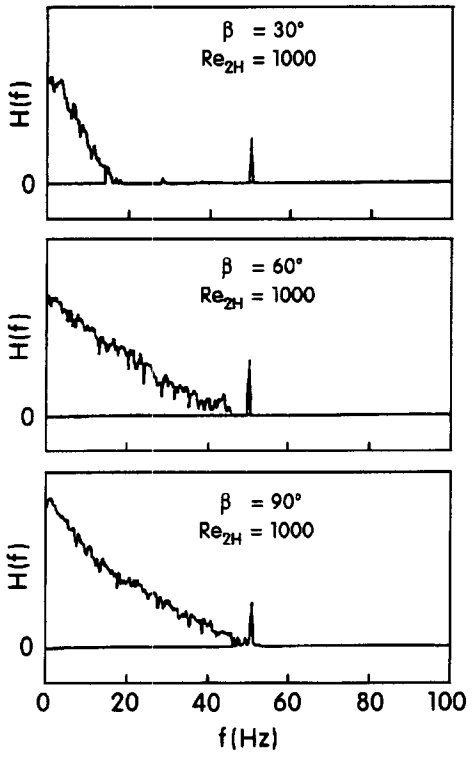

Figure 15 Measured frequency spectra for the same geometry as Figure 14 but at Re = 1000; $H(f)$ is the Fourier transform of the velocity; the position of the hotwire was at $P(3.6, 2, 0.125)$, from Riemann (1992)

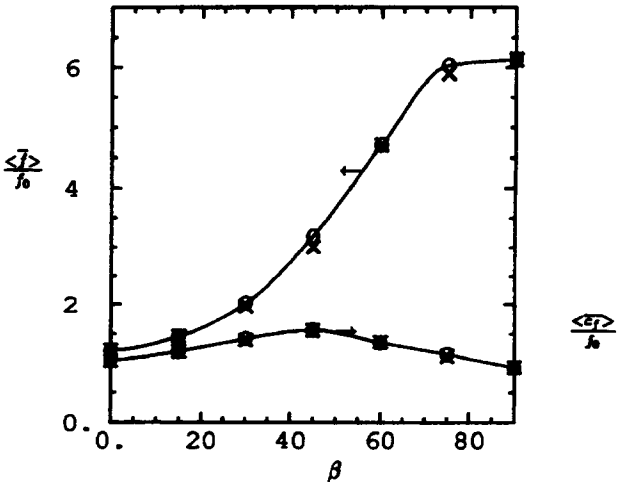

Figure 16 Time and area averaged normalized friction coefficient $(\bar{c}_f)/f_0$ and time and surface averaged apparent friction factor $\bar{f}/f_0$ as function of angle of attack for the configuration of Figure 3 at Re = 350; f_0, fully developed channel flow; *o*, periodic; *x*, symmetric side boundary conditions

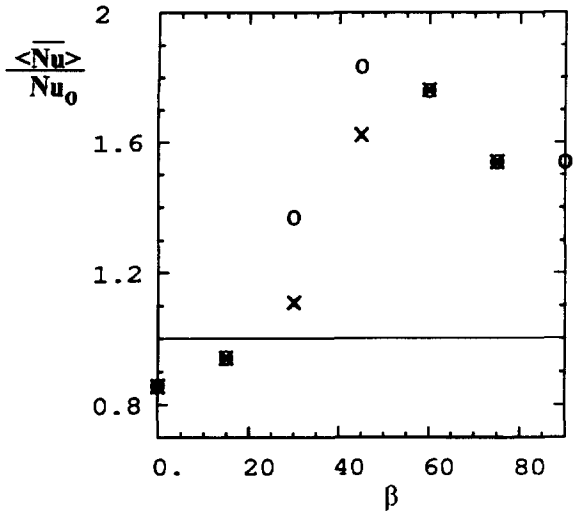

Figure 17 Time and area-averaged normalized Nusselt number Nu/Nu_0 as function of angle of attack β; *x*, symmetric side boundary conditions; 0, periodic side boundary conditions, for the configuration of Figure 16

and rectangular wings and winglets in the Reynolds number range between $2 \cdot 10^3$ and $8 \cdot 10^3$. His flow condition before the vortex generators was always laminar with a turbulence level of 0.78%. Behind the vortex generators, the turbulence increased to levels above 10% for Re > 2,200 (Figure 18). The hot-wire measurements were taken four channel heights behind the tip of the stamped delta winglets at half the channel height. The axial velocity profiles were also measured along the lateral direction for four Reynolds numbers. All axial velocity profiles show a deep minimum at the vortex core. This minimum value amounted to only 5% of the outer velocity for Re = 1,170 and became 20% for Re = 3,420. This is in contrast to the longitudinal vortices generated by a delta wing in external flow, where the axial velocity is nearly doubled in the core region. Only after vortex breakdown the axial velocity becomes very low, see Figure 1. This is a hint that vortex breakdown might have occurred. The turbulence level in the wake of the vortex generator changes from 1.5% at Re = 1,170, over 3% at Re = 1,660, to 11% at Re = 2,200, and 12% at Re = 3400. The high turbulence levels for Re > 2,000 indicate that the flow is in the transition regime. For Re = 4,600 and developing hydraulic and thermal conditions, the four wing-type vortex generators of Figure 2 were compared experimentally. The dimensions and parameters are given in

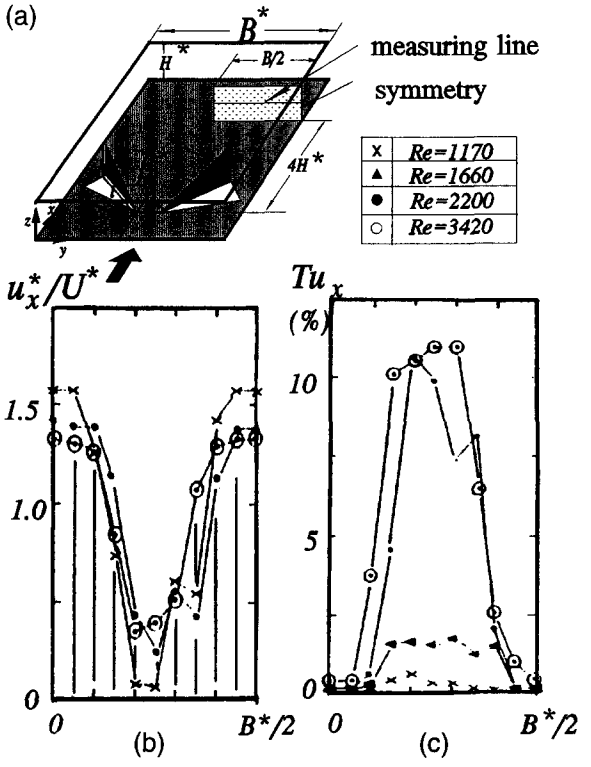

Figure 18 Flow behind a row of stamped delta winglets at 45° angle of attack at four different Reynolds numbers; (a) geometry of an element and measuring positions; (b) axial velocity profile; (c) turbulence level, from Tiggelbeck (1990)

Table 1. The rectangular winglet geometry is identical to that in Figure 3. The delta winglet and the delta wing have the same length and area as the rectangular winglet of Figure 3. The rectangular wing has the same area but a different length. The major difference between the geometry of Figure 3 and that described in Table 1 is the much larger area ratio $A_w/A_{VG} = 37.5$ compared to $A_w/A_{VG} = 10$ in Figure 3. Additional differences are the boundary conditions; Figure 3 implies periodically fully developed boundary conditions, while in the experiment, developing hydraulic and thermal conditions prevailed. Also, the measured drag is not the dissipation or pressure drop, because it does not include the velocity profile changes between entrance and exit; it corresponds to the apparant friction factor. The global

Table 1 Dimensions and parameters of the channel and wing-type vortex generators

Geometry of the channel					
Channel height	H^*, mm	20			
Width	B^*, mm	$5H^*$			
Length	L^*, mm	$15H^*$			
Vortex generator		**DW**	**DWP**	**RW**	**RWP**
Angle of attack	β°	30			
Trailing-edge width	b^*, $b^*/2$, mm	$2H^*$	H^*	$1.5H^*$	$0.5H^*$
Length	l^*, mm	$2H^*$	$2H^*$	$1.3H^*$	$2H^*$
Surface	A^*_{VG}, mm²	800	2 * 400	800	2 * 400
Aspect ratio	b^{*2}/A^*_{VG},	2	2	2.34	0.5
Surface ratio	A^*_W/A^*_{VG},	37.5			
Distance from the inlet	x^*_V, mm	H^*			
Reynolds number	Re,	4,600			

DW = Delta wing; DWP = Delta winglet pair;
RW = Rectangular wing; RWP = Rectangular winglet pair

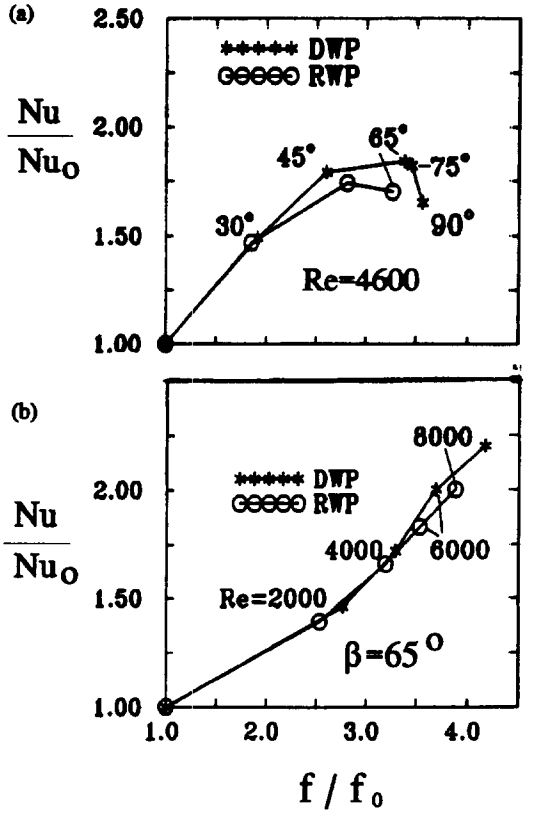

Figure 19 Mean Nusselt number enhancement Nu/Nu_0 over apparent friction factor penalty f/f_0 for (a) constant Re = 4600 and variable β and (b) constant β = 65° and variable Re, from Tiggelbeck (1990); Nu_0 and f_0 are the plane channel element values; geometry as in Table 1

values for Nusselt number, apparant friction factor, heat transfer, and drag enhancement are given in Table 2 for β = 30° and Re = 4,600. The experimental results can be summarized as follows: (1) stamped winglet configurations are superior to stamped wing configurations; and (2) the differences between rectangular and delta winglets are small.

Figure 19 shows the Nusselt number enhancement as a function of apparant friction factor with angle of attack and Reynolds number as parameters. The message of Figure 19 is: (1) for β ≥ 45° and Re ≥ 5,000, delta winglets perform slightly better than rectangular winglets; (2) both Nusselt number enhancement and apparant friction factor penalty increase with Reynolds number; and (3) the apparant friction factor increases monotonically with angle of attack, but the Nusselt number reaches a maximum at an angle of attack around 65°.

Table 2 Global Nusselt number and apparent friction factor for the channel with wing-type vortex generators. Geometry as in Table 1

	DW	DWP	RW	RWP
Nu	22.54	24.76	21.48	24.26
Nu/Nu_0	1.36	1.49	1.29	1.46
$f, 10^{-2}$	2.26	2.89	2.3	2.76
f/f_0	1.5	1.91	1.52	1.85
$(Nu/Nu_0)/(f/f_0)$	0.91	0.78	0.85	0.79

Re = 4600; $Nu_0 = 16.62$ (Shah & London, 1978); $f_0 = 1.52 * 10^{-2}$ (measured value); DW = Delta wing; DWP = Delta winglet pair; RW = rectangular wing; RWP = Rectangular winglet pair

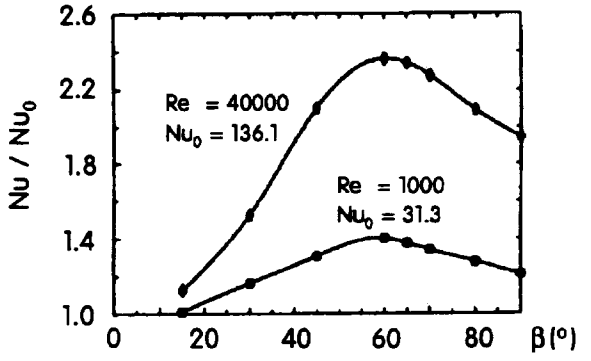

Figure 20 Mean heat transfer enhancement as function of angle of attack for $Re = 10^3$ and $40 \cdot 10^3$ for the geometry of Figure 3, from Riemann (1992). Fully developed flow but thermal entrance conditions, one wall adiabatic, one wall $\dot{q}$ = const., measurements by IRT; Nu_0 and f_0 are the values at β = 0

Turbulent flows

First, the one-sided constant heat flux results are discussed. The experiments were performed in the Reynolds number range $10^3 \leq Re \leq 40{,}000$ with fully developed flow conditions (Riemann 1992). Because of the continuous frequency spectrum at Re = 1,000, these conditions are also called turbulent. For the base configuration of Figure 3, the heat transfer enhancement and pressure penalty are shown in Figures 20 and 21 as functions of angle of attack for $Re = 10^3$, and $40 \cdot 10^3$. The values are nondimensionalized with the β = 0° data, which correspond to the channel with rectangular in-line fins aligned with the main flow direction. The reference values of the apparant friction factor f_0 and Nusselt number Nu_0 were measured. They depend on Re. In contrast, the reference condition for transitional flow was the channel without vortex generators. The major results here are that heat transfer enhancement increases up to β ≈ 60°, while the pressure loss increases monotonically up to β = 90° and that pressure loss and heat transfer enhancement increase with Re. Both are in general agreement with the results in the transition regime.

A quantitative comparison with the Re = 350 results could be misleading because of the different thermal boundary conditions. A quantitative comparison with the one row results at Re = 4,600 is useless, because the hydraulic and thermal boundary conditions are different. However, it should be mentioned that the results for Re = 350 show a higher heat transfer enhancement and lower increase in pressure loss than the results for Re = 1,000 shown in Figures 20 and 21. The $Re = 4 \cdot 10^4$ results for a periodic 10-row geometry and the $Re = 4.6 \cdot 10^3$ results for the 1-row geometry give about the same maximum heat transfer enhancement at

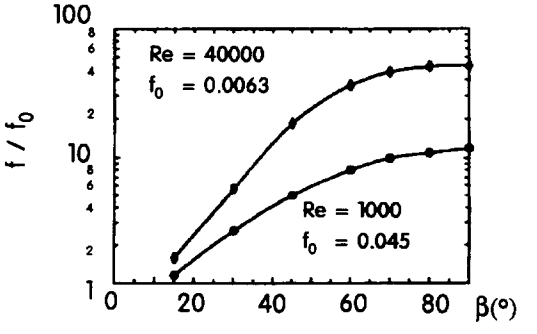

Figure 21 Pressure loss penalty for the conditions of Figure 20, from Riemann (1992)

Table 3 Channel with one row of vortex generators punched or attached to the upper wall, heat transfer enhancement Nu/Nu_0 and dissipation penalty $c_\varphi/c_{\varphi 0}$

	Nu/Nu_0, upper wall	Nu/Nu_0, lower wall	$c_\varphi/c_{\varphi 0}$
With punching	1.184	1.187	4.2
Without punching	1.20	1.177	4.2

$Nu_0 = 115$; $c_{\varphi 0} = 5.8 * 10^{-3}$

about the same angle of attack (60°), but the pressure loss enhancement is about a factor 10 lower for the 1-row configuration. The reason for the lower pressure loss penalty of the 1-row geometry stems partly from the fact, that the vortices increase heat transfer on an area 3.75 times larger than in the 10-row configuration, compare Figure 19 with Figures 20 and 21. The pressure loss penalty is however generated predominantly by the form drag of the vortex generators and increases strongly with Re for identical projected vortex generator area, so it should be much higher for $Re = 4 \cdot 10^4$ than for $Re = 4.6 \cdot 10^3$.

Zhu (1991) did numerical calculations for $Re \geqslant 10^5$ with geometries similar to Tiggelbeck's (1990) geometries. The numerical results for attached and stamped winglets are given in Table 3 for $\beta = 25°$ and Re = 100,000. The differences in heat transfer enhancement and pressure loss between punched and attached vortex generators are very small. Therefore, only attached delta winglets are considered further. Figure 22 shows the dependence of heat transfer and pressure loss on angle of attack. The dissipation and heat transfer increase monotonically with β up to the calculated β of 75°. Compared to the Re = 40,000 results of Riemann (1992), the heat transfer and pressure loss enhancement is considerably lower. The major reasons for the discrepancy are the different area ratios of 10 and 30, the different hydraulic and thermal conditions, and the different reference values. Riemann takes his own measurements at $\beta = 0°$ as reference. Zhu chooses values for the empty channel from the literature (Bhatti and Shah 1987) as reference. Zhu's element is 10H * long and 5H * wide, Riemann's is 5H * long and 4H * wide, and Zhu has hydrodynamically developing conditions, while Riemann has fully developed flow condition. However, Zhu also calculated conditions where the area ratio is similar to that used by Riemann. The plane channel values used by Zhu are

$$c_{fo} = 0.0868\ \mathrm{Re}^{0.25} \tag{11}$$

$$\mathrm{Nu}_0 = 5.8 + 0.02 \cdot \mathrm{Re}^{0.8} \cdot \mathrm{Pr}^{0.8} \qquad (T_w \text{ or } q_w = \text{const}) \tag{12}$$

The angle of attack and Reynolds number dependence of the heat transfer and dissipation enhancement for $A_w/A_{VG} = 10.4$ are given in Figures 23 and 24.

The Reynolds number dependence is shown for $\beta = 45°$ and the angle of attack dependence for $Re = 3 \cdot 10^5$. It is of interest to note: (1) the Reynolds number dependence of the heat transfer

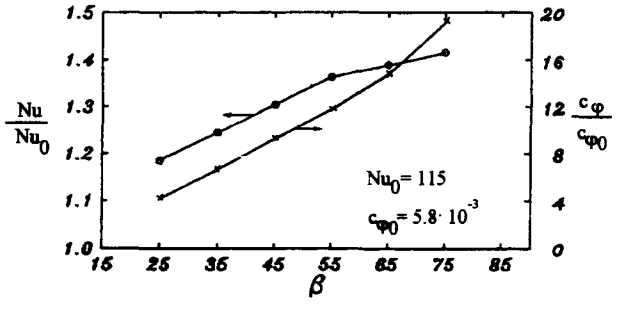

Figure 22 Enhancement of heat transfer and pressure loss as function of angle of attack for the delta winglet pair, from Zhu (1991); thermal entrance $T_W = 2 \cdot T_0$; $A_W/A_{VG} = 30$; Re = 100,000

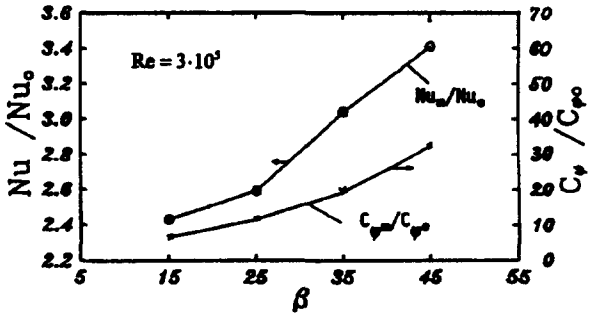

Figure 23 Calculated heat transfer and pressure loss enhancement for periodic rectangular winglets and fully developed conditions; smooth wall T_W = const., the wall with rectangular winglets is adiabatic, Zhu (1991); $A_W/A_{VG} = 10.4$; $L_P = 3.75$; $Re = 3 \cdot 10^5$; $l = 1.2$; $h = 0.6$; Pr = 0.2

enhancement becomes weaker for $Re \geqslant 10^5$, while this is not the case for the dissipation penalty; (2) the heat transfer enhancement increases less than the dissipation penalty with increasing angle of attack; and (3) for Re = 50,000 and $\beta = 45°$, the calculated heat transfer enhancement and dissipation penalty are slightly different from the measured values for Re = 40,000 and $\beta = 45°$.

Concluding remarks

Vortices are determined by the specific base flow and vortex generators. Developing and fully developed channel flows have been considered as base flow. Different wing types have been considered as vortex generators. They can easily be incorporated into heat transfer surfaces by embossing, stamping, or attaching them as fins to primary heat transfer surfaces. Wing-type vortex generators allow us to control the type and strength of the generated vortices by the form, area, and angle of attack of the wings. Vortices increase the rate of kinetic energy flux and dramatically change transition Reynolds number, temperature profiles, and their gradients at the wall. They enhance friction and heat transfer. The form drag of the vortex generator causes additional pressure loss.

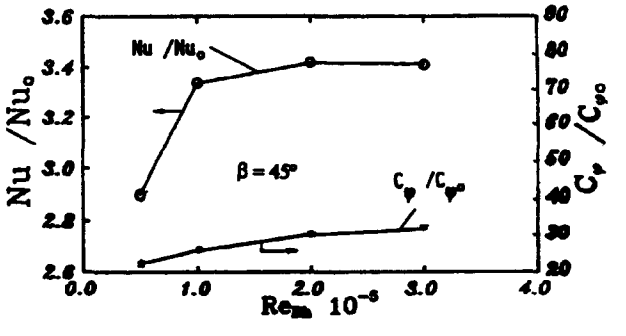

Figure 24 Heat transfer and pressure loss enhancement as function of Reynolds number for the conditions of Figure 23 and $\beta = 45°$, Zhu (1991)

For internal flows, the determination of the pressure loss penalty in relation to the heat transfer enhancement is important. Here, the generators are part of the heat transfer surface, and the pressure drop is mainly caused by the form drag of the vortex generators. Three enhancement mechanisms have been identified: (1) developing boundary layers on the vortex generator; (2) swirl or rotation of the flow; and (3) flow destabilization and unsteadiness. When the vortex generator area is small compared to the primary surface the developing boundary layers on the vortex generator have only a minor effect. Strong cross-flow generated by longitudinal vortices always makes a major contribution to heat transfer enhancement. Destabilization of the developed velocity profile by vortices leads to a drastic reduction of the critical Reynolds number by up to two orders of magnitude; for the ribbed channel $\beta = 90°$, the critical Reynolds number is reduced to $Re < 200$, so a flow at $Re = 350$ is already transitional. However, the "swirl" and "destabilization" effect cannot be separated in turbulent or transitional flow. The separation of the two effects was only possible by the trick of imposing different side boundary conditions, which made the flow steady or unsteady for the same Re.

Different wing-type vortex generators and thermal and hydraulic boundary conditions were considered. As a base configuration, periodic rectangular, attached vortex generators with $h = 0.5$, $1 = 2$ and an area ratio $A_w/A_{VG} = 10$ have been investigated for varying Reynolds numbers and angles of attack. The major results are as follows.

- Vortices can reduce the critical Reynolds number by a factor of 10 and more.
- Longitudinal vortices give higher heat transfer enhancement than transverse vortices, for the same pressure loss penalty.
- Wing-type vortex generators are easy to integrate into heat transfer surfaces and are effective vortex generators.
- Compared to wings, winglets produce the same heat transfer enhancement for less pressure penalty.

Further studies are needed to optimize wing-type vortex generators for different heat transfer situations.

Acknowledgment

The generous financial support of the Deutsche Forschungsgemeinschaft (DFG) is gratefully acknowledged.

References

Bhatti, M. S. and Shah, R. K. 1987. Turbulent and transition flow convective heat transfer in ducts. In *Handbook of Single-Phase Convective Heat Transfer*, S. Kakac et al. (eds.), Wiley, New York

Bergles, A. E. and Webb, R. L. 1985. A guide to the literature on convective heat transfer augmentation. *Advances in Heat Transfer, 23rd Natl. Heat Transfer Conference*, Denver, CO

Delerey, J., Horowitz, E., Leuchter, O. and Solignac, J. -L. 1984. Fundamental studies on vortex flow. *La Recerche Areospatiale.* **2**, 1–24

Donne, M. D. and Meyer, L. 1977. Turbulent convective heat transfer from rough surfaces with two-dimensional rectangular ribs. *Int. J. Heat Mass Transfer.* **20**, 583–620

Drazin, P. G. and Reid. W. H. 1984. Hydrodynamic Stability. Cambridge University Press, Cambridge, UK

Eibeck, P. A. and Eaton, J. K. 1986. The effects of longitudinal vortices embedded in a turbulent boundary layer. *Proc. 8th IHTC*, Vol. 3, S. 1115–1120, San Francisco

Fiebig, M., Kallweit, P. and Mitra, N. K. 1986. Wing-type vortex generators for heat transfer enhancement. IHTC, **6**, 2909–2913

Fiebig, M., Kallweit, P., Mitra, N. K. and Tiggelbeck, S. 1991. Heat Transfer enhancement and drag by longitudinal vortex generators in channel flow. *ETF-Sience*, **4**, 103–114

Fiebig, M. 1993. Vortex generators for compact heat exchangers. *Proc. Int. Symposium on New* Developments in Heat Exchangers, ICHMT, 5.-8.9. 1993, Portugal

Ghaddar, N. K., Korczak, K. Z., Mikic, B. B. and Patera, A. T. 1986. Numerical investigation incompressible flow in grooved channels, Part I, Stability and self-sustained oscillations. *J. Fluid Mechanics*, **163**, 99–127

Grosse-Gorgemann, A., Weber, D. and Fiebig, M. 1993. Numerical and experimental investigation of self-sustained oscillations in channels with periodic structures. *Proc. Eurotherm, 31*, Bochum, Germany, 42–50

Grosse-Gorgemann, A., Weber, D., Mitra, N. K. and Fiebig, M. 1994. Selbsterregte Schwingungen in Kanalströmungen mit Wirbelerzeugern: Experiment und Numerik. *GAMM-Tagung 1994, Braunschweig*

Güntermann, T. 1992. Dreidimensionale stationäre und selbsterregtschwingende Strömungs- und Temperaturfelder in Hochleistungswärmeübertragern mit Wirbelerzeugern. *VDI-Fortschrittsberichte, Reihe 19 Nr. 60*

Han, J. C., Glicksmann, L. R. and Rosehnow, W. M. 1978. An investigation of heat transfer and friction for rib-roughened surfaces. *Int. J. Heat Mass Transfer*, **21**, 1143–1156

Hanjalic, K. and Launder, B. E. 1972. Fully developed asymmetric flow in plane channel. *J. Fluid Mechanics*, **51**, 301–335

Hummel, D. 1979. On the vortex formation over a slender wing at large angels of incidence. 4GARD-CP-247

Kakac, S., Shah, R. K. and Aung. W. 1987. *Handbook of Single-Phase Heat Transfer*. Wiley, New York, 3–42

Kallweit, P. 1986. Längswirbelerzeuger für den Einsatz in Lamellenwärmetauschern. Ph.D. thesis, Ruhr-Universität Bochum, Germany

Karniadakis, G. E., Mikic, B. B. and Patera, A. T. 1987. Minimum-dissipation transport enhancement by flow destabilisation: Reynolds' analogy revisted. *J. Fluid Mech.*, **192**, 365–391

Kost, A., Mitra, N. K. and Fiebig, M. 1992. Calculation procedure for unsteady incompressible 3-D flows in arbitrarily shaped domains In *Notes of Numerical Fluid Mechanics*, Vol. 35, Vieweg-Verlag, 269–278

Kozlu, H., Mikic, B. B. and Patera, A. T. 1988. Minimum-dissipation heat removal by scale-matched flow destabilization, *Int. J. Heat Mass Transfer*, **31**, 2023–2032

Launder, B. E. and Spalding, D. B. 1974. The numerical computation of turbulent flows. *Comp. Methods Appl. Mech. Eng.*, **103**, 269–289

Leibovich, S. 1984. Vortex stability and breakdown, survey and extension. *AIAA J.*, **22**, 1192–1206

Merker, G. P. 1987. *Konvektive Wärmeübertragung*. Springer-Verlag, Berlin, 412

Müller, U. 1993. Strömungsstruktur bei periodischer Anordnung von Rippenstrukturen bei einem Anstellwinkel von $\beta = 0°$-$75°$. Studienarbeit Nr. 93/15, Ruhr-Universität Bochum

Müller, U. 1994. Wärmeübergang und Druckverlust bei Hochleistungswärmeübertragungsflächen mit periodischen Wirbelerzeugern. Bedeutung von Anstellwinkel und Randbedingungen. Diplomarbeit Nr. 94/8, Ruhr-Universität Bochum

Riemann, K. -A. 1992. Wärmeübergang und Druckabfall in Kanälen mit periodischen Wirbelströmungen bei thermischem Anlauf. Ph.D. thesis, Ruhr-Universität Bochum, Germany

Sarpkaya, T. 1989. Computational methods with vortices — The 1988 Freeman scholar lecture. *J. Fluids Eng.* **III**, 5–52

Schäfer, P. and Herwig, H. 1993. Drag and heat transfer in laminar boundary layers with finite regions of separation. *Proc. Eurotherm 31*, Bochum, Germany, 17–22

Tiggelbeck, S. 1990. Experimentelle Untersuchungen an Kanalströmungen mit Einzel- und Doppel-Wirbelerzeuger-Reihen für den Einsatz in kompakten Wärmetauschern. *VDI-Fortschrittsberichte*, Reihe 19, Nr. 49

Tiggelbeck, T., Mitra, N. K. and Fiebig, M. 1993. Experimental investigations of heat transfer and flow losses in a channel with double rows of longitudinal vortex generators. *Int. J. Heat Mass Transfer*, **36**, 2327–2337

Trefethen, L. M. and Panton, R. B. 1990. Some unanswered questions in fluid mechanics. *Appl. Mech. Rev.*, **110**, 175–183

Van Dyke, 1988. *An Album of Fluid Motion.* The Parabolic Press. Stanford, CA

Webb, R. L. 1987. Enhancement of single-phase heat transfer. In *Handbook of single-phase convective heat transfer*, S. Kakac et al. (eds.) Wiley, New York

Zhang, Z. 1989. Einfluß von Deltaflügel-Wirbelerzeugern auf Wärmeübergang und Druckverlust in Spaltströmungen, Ph.D. thesis, Ruhr-Universität Bochum, Germany

Zhu, J. X. 1991. Wärmeübergang und Strömungsverlust in turbulenten Spalströmungen mit Wirbelerzeugern. *VDI-Fortschrittsberichte,* Reihe 7, Nr. 192

Zhu, J. X., Mitra, N. K. and Fiebig, M. 1993. Effects of longitudinal vortex generators on heat transfer and flow loss in turbulent channel flows. *Int. J. Heat Mass Transfer*, **36**, 2339–2347

Zhu, J. X., Mitra, N. K. and Fiebig, M. 1994. Turbulent flow and heat transfer in a channel with longitudinal vortex generators and rib-roughened wall. Submitted to ASME-WAM, 1994, Chicago